

The Analysis, Synthesis, and Evaluation of Local Measures For Discrimination and Segmentation of Textured Regions

James Crowley and Alice Parker

Department of Electrical Engineering
Carnegie-Mellon University

ABSTRACT:

Textured regions pose problems for segmentation algorithms whether they are based on boundary detection or thresholding techniques. First order statistical measures based on local measures of gray level patterns (local properties) can be used as features for segmentation or for classification of textured regions.

An analysis technique for local properties is described. Several local properties for measuring the graininess and directionality of a textured region are presented, analysed, and evaluated on a set of test images. The results of the analysis procedure are verified by comparison with the performance on test images.

1.1 The Concept of Image Texture

When a region of an image contains many rapid fluctuations in intensity, such a region is sometimes said to be "textured". Interest in image texture has often been motivated by the difficulties which such regions pose for image segmentation systems.

Image "texture" is a perceptual phenomenon. A human observer is capable of grouping areas of a picture in which the patterns of fluctuations are similar into individual regions and can even draw a boundary about such regions. However, the mechanisms of human visual perception are not well understood and thus it is not possible to specify the measures by which a human defines a textured region.

Often the term texture has been used to denote some particular ad-hoc measure of the variations in light and/or color intensity of an image. Such measures have been described in the literature for tasks such as:

- 1) Classifying an entire image [Haralick, et al, 1973];
- 2) Identifying regions of an image which are too "busy" to classify on the basis of color features [Ohlander, 1975]; and
- 3) Segmenting an image into regions of uniform variations in gray level and/or color ([Rosenfeld, 1969]) and [Bajcsy, 1973] among others.

This paper presents a general purpose technique for segmenting and/or classifying regions of an image.

We consider an image to be a two-dimensional signal, and apply digital signal processing techniques to derive a set of measures for detecting and classifying events in an image.

In chapter two we will describe the use of the transfer function to characterize the properties of a linear function. The transfer function can be used to analytically characterize the image signals to which most edge detection operators are sensitive, even when the operator is a non-linear combination of linear functions.

In chapter three we derive a family of linear functions which detect image properties at various resolutions and orientations. This family of functions is tuneable to any level of angular discrimination.

In chapter four we demonstrate how these functions may be used to detect various classes of cells in liver tissue biopsy images, regardless of the bias and gain at which the image was recorded. We also show how these functions may be used to segment out dense regions of a particular cell type.

2.1 Linear Local Properties And Their Transfer Functions

Many image analysis procedures for tasks such as boundary detection, texture segmentation or planning, are based on finite discrete two-dimensional linear functions. In this section we shall be concerned with an analytic technique for characterizing the response of a linear function to an image. This technique is based on the fact that such linear functions are mathematically equivalent to two dimensional finite impulse response digital filters.

Consider a linear function defined by a finite two-dimensional $2M+1$ by $2N+1$ array of coefficients (or point spread function) $h(m,n)$. To simplify our notation we will illustrate our discussions with point spread functions with an odd number of rows and columns, and denote the center point as $(0,0)$. The value produced by this linear function, $L(x_0, y_0)$, at a $2M+1$ by $2N+1$ neighborhood of the discrete picture function, $P(x,y)$, centered at (x_0, y_0) , is given by equation 2.1.

$$L(x_0, y_0) = \sum_{m=-M}^M \sum_{n=-N}^N h(m,n)P(x_0+m, y_0+n) \quad (2.1)$$

An interesting property of linear functions is the existence of eigenfunctions or characteristic

functions. When a linear function is measured over one of its eigenfunctions, the sequence that results will be the same eigenfunction scaled in amplitude and shifted in phase. The eigenfunctions of two-dimensional linear functions are the complex exponentials (eq. 2.2), where u and v are continuous variables which we shall refer to as spatial frequencies.

$$e^{\pm j(xu+yv)} = \cos(xu+yv) \pm j \sin(xu+yv) \quad (2.2)$$

The sequence which results from measuring the linear function over a complex exponential is shown in equation 2.3.

$$L(x,y) = \sum_{m=-M}^M \sum_{n=-N}^N h(m,n) e^{j[(m+x)u + (n+y)v]} \\ = H(e^{ju}, e^{jv}) e^{j(xu + yv)} \quad (2.3)$$

The function $H(e^{ju}, e^{jv})$, which is referred to as the transfer function of the linear function, specifies an amplitude scaling and position shift which relates the resulting sequence to the input sequence.

A linear function of a sum of complex exponentials results in a sum of the same exponentials, with each complex exponential scaled and shifted individually, as shown in eq. 2.3. Since any two dimensional discrete signal may be unambiguously represented by a weighted sum of complex exponentials, the transfer function of a linear function completely characterizes the effect that linear function will have on any two-dimensional discrete signal.

The transfer function for a given linear function is formed as a Fourier series expansion in the frequency domain using the point spread function coefficients, $h(m,n)$. For a discrete point spread function the transfer function will be a periodic function of the frequencies u and v , with a period of 2π .

We may derive the formula for computing the transfer function of a point spread function from the eq. 2.3 by factoring out the component of the complex exponential which is not a function of the summation variables, m and n , as shown in eq. 2.4.

$$L(x,y) = e^{j(xu+yv)} \sum_{m=-M}^M \sum_{n=-N}^N h(m,n) e^{j(mu+nv)} \\ = H(e^{ju}, e^{jv}) e^{j(xu + yv)} \quad (2.4)$$

By eliminating like terms in eq. 2.4 we see that the transfer function is given by eq. 2.5.

$$H(e^{ju}, e^{jv}) = \sum_{m=-M}^M \sum_{n=-N}^N h(m,n) e^{j(mu + nv)} \quad (2.5)$$

A polynomial representation of $H(e^{ju}, e^{jv})$ for reasonably short duration point spread functions may be formed quite simply with paper and pencil. The variables of this polynomial are the functions $\cos(xu + yv)$ and $j \sin(xu + yv)$, which are related

to the complex exponential as shown in eq. 2.2.

Recall that any sequence can be decomposed into a sum of a symmetric, or even, sequence and an anti-symmetric, or odd, sequence. Let us define the even part of $h(m,n)$ as $e(m,n)$ as shown in eq. 2.6 and the odd part of $h(m,n)$ as $o(m,n)$ as shown in eq. 2.7.

$$e(m,n) = h(m,n) + h(-m,-n) \quad (2.6)$$

$$o(m,n) = h(m,n) - h(-m,-n) \quad (2.7)$$

By substituting the identity shown in eq. 2.2 into the formula for the transfer function, eq. 2.5, and then substituting eqs. 2.6 and 2.7 we arrive at a formula for the transfer function as a sum of Cosine and Sine terms as shown in eq. 2.8.

$$H(e^{ju}, e^{jv}) = h(o,o) + \sum_{m=1}^M \sum_{n=1}^N e(m,n) \cos(xu+yv) + j o(m,n) \sin(xu+yv) \quad (2.8)$$

For point spread functions in which there are an even number of rows (or columns) the center point will fall between samples causing the values of n (or m) to be odd multiples of $\frac{1}{2}$ and the $h(o,o)$ term to be zero.

As an example of the derivation of a transfer function, consider the point spread function shown in eq. 2.9 which is a component of the sobel edge detector [Duda and Hart, 1971].

$$h(m,n) = \begin{bmatrix} 1 & 2 & 1 \\ 0 & 0 & 0 \\ -1 & -2 & -1 \end{bmatrix} \quad \text{for } -1 \leq m, n \leq 1 \quad (2.9)$$

Since this point spread function is anti-symmetric about its center point, its even part is identically zero. Its odd part is listed in eq. 2.10.

$$\begin{aligned} o(1,1) &= 2 \\ o(0,1) &= 4 \\ o(-1,1) &= 2 \\ o(1,0) &= 0 \end{aligned} \quad (2.10)$$

Thus the transfer function of this point spread function is a simple sum of three imaginary Sine functions as shown in eq. 2.11.

$$H(e^{ju}, e^{jv}) = 2j \sin(u+v) + 4j \sin(v) + 2j \sin(-u+v) \quad (2.11)$$

An orthographic projection of this transfer function is shown in Figure 2.1.

The transfer function can be a powerful analytic tool for describing picture processing operators which are composed of linear functions [Parker and Crowley, 1978].

The formula for computing a linear function, $L(x,y)$, shown in eq. 2.1 is often referred to as the cross correlation of $h(m,n)$ with $p(x,y)$, and denoted $c_{hp}(x,y)$. This formula is also equivalent to the inner product of $h(m,n)$ and the values in the $2M+1$

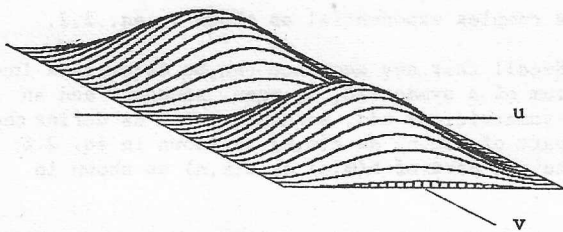


Figure 2.1 Transfer Function of Component of Sobel Edge Detector

by $2N+1$ neighborhood of $p(x,y)$ centered at each point (x,y) , denoted $\langle h,p(x,y) \rangle$. These equivalent formulas are shown in eq. 2.12.

$$C_{hp}(x,y) = \langle h,p(x,y) \rangle = \sum_{m=-M}^M \sum_{n=-N}^N h(m,n)p(x+m,y+n) \quad (2.12)$$

3.0 Synthesis of a Family of Linear Functions Object Detection or Region Segmentation

In some scene analysis problems much of the image data is composed of many instances of a class of small objects for which the precise shape, size and distance between objects varies randomly. We have designed a family of linear functions which may be used to classify regions of such an image. These functions may also be tuned to detect objects with a given range of widths and/or a particular range of orientations. In this section we will describe the specification of these functions and then design an analytic (but non-optimal) implementation based on the Kaiser low pass window function [Kaiser, 1974].

3.1 The Sampling Theorem and Band-Limited Functions.

In most cases, the segmentation and classification of regions requires that image signal properties be measured over a range of resolutions. However, the size of a point spread function must be larger than the signal property which it is to detect, and computing the cross correlation, $C_{hp}(x,y)$, at each image point can require a prohibitive number of multiplications and additions if the point spread function is large. Fortunately, it is possible to design point spread functions for detecting large image properties which may be measured at a fixed interval without loss of information.

When we compute the cross correlation $C_{hp}(x,y)$, we are, in effect sampling $C_{hp}(x,y)$ at these intervals. The rate at which $C_{hp}(x,y)$ may be sampled is governed by the sampling theorem [Oppenheim and Schaffer, 1975]

Undersampling may result in aliasing, a phenomenon

* In eqs. 2.1 and 2.2 we have neglected the boundary effects which result from the fact that the picture function, $p(x,y)$, is only defined for a finite range of x and y , say $0 \leq x \leq X-1$ and $0 \leq y \leq Y-1$. In fact, the values of $C_{hp}(x,y)$ will only be meaningful when the neighborhood defined by $h(m,n)$ is contained completely within the picture function, i.e. for $0 \leq x \leq X-2M-2$ and $0 \leq y \leq Y-2N-2$.

in which frequency components greater than one half cycle per sample (the Nyquist Rate) are "folded" over the Nyquist Rate and appear as signal components with lower frequencies. Thus, if we measure $C_{hp}(x,y)$ at intervals of more than one column and one row (i.e. $S_x, S_y > 1$), we introduce an error which is proportional to sum of the signal energy in $C_{hp}(u,v)$ for $1/S_x < |u| < 1/2$ or $1/S_y < |v| < 1/2$.

The Fourier transform of the cross correlation, $C_{hp}(u,v)$, is equal to the product of $H(e^{ju}, e^{jv})$ and the Fourier transform of the picture function, $P(u,v)$. Thus, to limit the signal energy in $C_{hp}(u,v)$ for frequencies greater than $1/S_x$ and $1/S_y$ we must design $h(m,n)$ so that $H(e^{ju}, e^{jv})$ is small within this region.

It is not possible for a point spread function of finite non-zero extent (i.e. space limited) to have a transfer function which is identically zero over any significant two dimensional region of the frequency plane. [Slepian and Pollack, 1961] and [Landau and Pollack, 1961]. However, it is possible to design linear functions for which the magnitude of the transfer function is below an arbitrary constant, δ , outside of a specific pass region.

The design of optimal (minimum error) digital FIR filters requires iterative design algorithms such as the Parks-McClellan Algorithm. [McClellan et al., 1973]. However, to illustrate our approach without the cost of developing such software we have experimented with the design of two-dimensional FIR filters based on low pass window functions.

A particularly flexible family of low pass window functions is given by the Kaiser window. [Kaiser, 1974]. The formula for a Kaiser window is shown in eq. 3.1, in which β is a shape parameter which is determined by the stop-band attenuation, A_t , r is the distance from the center point of the filter, M is the maximum value of r for which the filter is non-zero, and I_0 is the zeroth order modified Bessel function of the first kind.

$$\omega(r) = \frac{I_0(\beta \sqrt{1 - (r/M)^2})}{I_0(\beta)} \quad (3.1)$$

The Kaiser window is a closed form approximation to the prolate spheroid wave functions [Rabiner and Gold, 1975] which are the eigenfunctions of band-limited space-limited linear functions [Landau and Pollack, 1971]. For a Kaiser Window, the parameters of window duration, $2M+1$, minimum stop-bound attenuation, $A_t := -20 \log_{10} \delta$, and transition width, Δf , are related by eq. 3.2.

$$\Delta f = \frac{A_t - 7.95}{28.72} \quad (3.2)$$

In section 3.2 we will derive a family of two-dimensional linear functions for which the duration of the point spread function in each direction, (x,y) , is inversely related to the upper edge of the

pass region in that direction. Thus for this family of functions the sample rates, S_x and S_y , are proportional to the length of the sides of the minimum rectangle which encloses the point spread function, $2N+1$ and $2M+1$. The result is that the cost, C , as measured by the number of number of multiplications for computing a sampled cross correlation is constant, as shown in eq. 3.3, regardless of the point spread function size.

$$C = 0 \left[\frac{(2N+1)(2M+1) \cdot X \cdot Y}{S_x \cdot S_y} \right] \quad (3.3)$$

where $O[]$ denotes "on the order of"

In fact, the actual cost is somewhat less than as is shown in eq. 3.3 because the point spread functions are ellipses bounded by a rectangle whose sides are $2N+1$ and $2M+1$.

3.2 Derivation of a Family of Two-Dimensional Linear Functions

The Kaiser Window, eq. 3.1, may be used to design a two dimensional Low Pass FIR digital filter which is circularly symmetric by substituting the euclidean distance from the center of the point spread function for the distance variable r in eq. 3.1 as shown in eq. 3.4 [Rabiner and Gold, 1974].

$$r^2 = x^2 + y^2 \quad (3.4)$$

We have found that a low pass FIR digital filter for which the lines of constant frequency response in the pass band are ellipses may be derived by substituting the equation of an ellipse, eq. 3.5, for the distance variable r .

$$r^2 = Ax^2 + Bxy + Cy^2 \leq M_R^2 \quad (3.5)$$

The coefficients for the ellipse polynomial may be derived from the length of the major axis, $2M_a+1$, the length of the Minor axis, $2M_i+1$, and the orientation of the major axis, θ , by the relations shown in eq. 3.6.

$$e^2 := 1 - \frac{M_i^2}{M_a^2}$$

$$A = 1 - e^2 \cos^2(\theta)$$

$$B = -2e^2 \cos(\theta) \sin(\theta) \quad (3.6)$$

$$C = 1 - e^2 \sin^2(\theta)$$

$$M_R^2 = M_a^2 (1 - e^2)$$

The variable M_R^2 is used for the variable M^2 in the Kaiser Window formula, eq. 3.1, so that the elliptical low pass window is given by eq. 3.7.

$$\omega(x,y) = \frac{I_0(\beta \sqrt{1 - \frac{Ax^2+Bxy+Cy^2}{M_R^2}})}{I_0(\beta)} \quad (3.7)$$

The shape parameter, β , for a Kaiser Window is determined by the minimum stop band attenuation, A_t , usually computed from eq. 3.2. The relationship between β and A_t is given by eq. 3.8.

$$\beta = \begin{cases} 0 & \text{for } A_t < 21 \\ .5842(A_t - 21)^{0.4} + .07886(A_t - 21) & \text{for } 21 \leq A_t \leq 50 \\ .1102(A_t - 8.7) & \text{for } A_t > 50 \end{cases} \quad (3.8)$$

To compute the attenuation A_t for a low pass ellipse filter we substitute the value M_R for M in eq. 3.2.

To create the coefficients for an orientation selective band-pass filter, $h_{f_c \phi}(x,y)$, from an elliptical low pass window, we multiply the low pass point spread function by a cosine with a specific direction, ϕ , and frequency, f_c , as shown in eq. 3.9.

$$h_{f_c \phi}(x,y) = \omega(x,y) \cdot \cos(r \cdot \cos(\alpha) \cdot 2\pi f_c)$$

where: $r = \sqrt{x^2 + y^2}$ (3.9)

and $\alpha = \phi - \tan^{-1}(\frac{y}{x})$

An example of the transfer function of an elliptical band-pass filter designed with this method is shown in Figure 3.1.

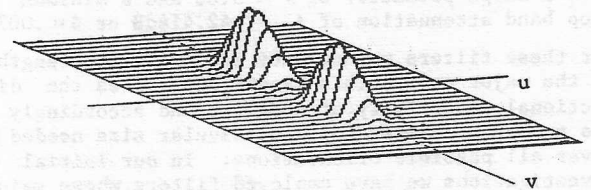


Figure 3.1 Transfer Function of an Elliptical Band Pass Filter

$M_i=6$, $M_a=9$, $\phi=90^\circ$, $\theta=0^\circ$, $f_c=.15$ samples/cycle
 $\Delta f=.20$.

As shown in Figure 3.1, the cosine is oriented along the minor axis. Because there is an inverse relationship between the duration of a point spread function of an ellipse in a given direction and the width of its pass region in that direction [Papoulis, 1968], multiplying by a cosine along the minor axis results in a band-pass filter with the major axis of its transfer function pass region extending radially from the origin of the u,v plane.

To complete the design of our family of filters requires that we specify criteria which relate the frequency of the cosine, f_c , to the duration of the minor axis of the point spread function. Since image events are usually not periodic it was decided to restrict the cosine frequency so that less than two cycles appear across the minor axis of the point spread function. Thus the center frequency, f_c , of a given filter is related to the duration of the

minor axis of the point spread function by eq.3.10, where λ_c is the wavelength of the cosine.

$$\frac{2}{f_c} = 2\lambda_c > 2M+1 \quad (3.10)$$

By experimentation we have observed that when $2/f_c \approx 2M$, good stop band characteristics may be achieved by letting $\Delta f = 4f_c/3$, provided that M is greater than 4. For such values of f_c and Δf , the width between the center point of the pass region and the zero crossing is approximately $f_c/2$. We label this effective transition width as Δf_e and note this is the value which we shall use to compute the sampling rates for a filter. However, to compute the shape parameter, β , for a filter we use the relation, $\Delta f = 4f_c/3$. Since we desire that the sampling rates be integers we constrain the sum of f_c and Δf_e so that they are integer fractions of the Nyquist rate. These relations are summarized in eq. 3.11.

$$M_i = 1/f_c - 1/2$$

$$\Delta f = \frac{\Delta f_e}{2} = \frac{4}{3} f_c \quad (3.11)$$

$$f_c + \Delta f_e = \frac{5}{3} f_c = \frac{1}{k} \cdot \frac{1}{2} \text{ for } k = 1, 2, 3, \dots$$

For Filters designed to these specifications we have a shape parameter of $\beta = 3.68$ and a minimum stop band attenuation of $A_c = -42.414\text{dB}$ or $\delta = .0075$.

For these filters we have not specified the length of the major axis. This length determines the directional sensitivity of a filter and accordingly the number of filters of a particular size needed to cover all possible orientations. In our initial investigations we have employed filters whose major and minor axis are equal so that 4 filters are required to detect events at all orientations.

We have found by experimentation that a sum of four filters may be used to form a circularly symmetric band-pass filter. The construction begins by forming a circularly symmetric Kaiser low-pass filter for which $M_i = M_a$ and $\Delta f = 4/3 f_c$ as described above. Four copies of this low pass filter are then multiplied by cosines of frequency f_c and orientations of $\phi=0^\circ, 45^\circ, 90^\circ$, and 135° . The sum of these four filters is a close approximation of a circularly symmetric band-pass filter whose transfer function contains a pass region which is a ring of center frequency f_c and width $f_c/2$. The minimum stop-band attenuation is 4dB greater than that of the individual filters. Thus for $\beta = 3.68$, $A_c = -42.414 + 4\text{dB} = -38.414\text{dB}$ and $\delta = .0075 \times 4 = .030$. A plot of the transfer function for a circularly symmetric band pass filter for which $f_c = .15$ and $M_i=M_a=6$ is shown in Figure 3.2 below.

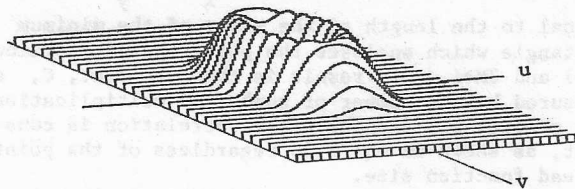


Figure 3.2 Transfer Function of Circularly Symmetric Band Pass Filter for which $f_c = .15$, $\Delta f = .20$, $M_i = M_a = 6$.

4.0 Experimental Evaluation

In this section we describe three simple experiments in which the filters derived in section 3 are used to detect classes of objects. The three 128×128 test images for these experiments, shown at the top of figure 4.1, have 256 grey levels. The first is an artificial image of circles of radius 6 and 8, with intensity 128 on a background of 64. Our task for this image is to detect the circles of radius 6 while avoiding the circles of radius 8.

The second test image is an artificial image containing a "herring bone" pattern. This pattern is composed of line segments of width 4, length 16, and a separation of 4 oriented at 45° and -45° . The pattern is of intensity 128 on a background of 32. The task for this image is to detect the -45° bars.

The third test image is taken from a digitized liver tissue biopsy image. Our task for this image is to detect the small dark nuclei of leukocytes and other cells in an inflammatory region at the top of the image while avoiding the nuclei of hepatic (liver) cells which are somewhat larger but often equally dark.

The filters used in these experiments have been normalized for a peak gain of 1 by dividing the point spread function by the square root of the sum of the squares of the coefficients. Prior to the computation of a correlation the mean and standard deviation of the picture points within the image are computed. During the computation of the correlation, as each picture element is read, it is converted to a 32 bit floating point number, the mean is subtracted, and the difference is multiplied by one over the standard deviation. Thus the resulting correlation is independent of the bias and gain at which the image was recorded.

The result of each sampled cross correlation is an array of floating point numbers. The maximum and minimum values in this array are determined and this range is divided into 256 bins, with the most negative value assigned to bin 0 and the most positive value assigned to bin 255. An integer block is then constructed in which the bin number from each value in the sampled correlation is written in a rectangle. The length of the sides of this rectangle are the horizontal and vertical sample rates (S_y and S_x). The rectangle is centered at the point at which that sampled correlation value was measured.

minor axis of the point spread function by eq.3.10, where λ_c is the wavelength of the cosine.

$$\frac{2}{f_c} = 2\lambda_c > 2M+1 \quad (3.10)$$

By experimentation we have observed that when $2/f_c \approx 2M$, good stop band characteristics may be achieved by letting $\Delta f = 4f_c/3$, provided that M is greater than 4. For such values of f_c and Δf , the width between the center point of the pass region and the zero crossing is approximately $f_c/2$. We label this effective transition width as Δf_e and note this is the value which we shall use to compute the sampling rates for a filter. However, to compute the shape parameter, β , for a filter we use the relation, $\Delta f = 4f_c/3$. Since we desire that the sampling rates be integers we constrain the sum of f_c and Δf_e so that they are integer fractions of the Nyquist rate. These relations are summarized in eq. 3.11.

$$M_i = 1/f_c - 1/2$$

$$\Delta f = \frac{\Delta f_e}{2} = \frac{4}{3} f_c \quad (3.11)$$

$$f_c + \Delta f_e = \frac{5}{3} f_c = \frac{1}{k} \cdot \frac{1}{2} \text{ for } k = 1, 2, 3, \dots$$

For Filters designed to these specifications we have a shape parameter of $\beta = 3.68$ and a minimum stop band attenuation of $A_c = -42.414\text{dB}$ or $\delta = .0075$.

For these filters we have not specified the length of the major axis. This length determines the directional sensitivity of a filter and accordingly the number of filters of a particular size needed to cover all possible orientations. In our initial investigations we have employed filters whose major and minor axis are equal so that 4 filters are required to detect events at all orientations.

We have found by experimentation that a sum of four filters may be used to form a circularly symmetric band-pass filter. The construction begins by forming a circularly symmetric Kaiser low-pass filter for which $M_i = M_a$ and $\Delta f = 4/3 f_c$ as described above. Four copies of this low pass filter are then multiplied by cosines of frequency f_c and orientations of $\phi=0^\circ, 45^\circ, 90^\circ$, and 135° . The sum of these four filters is a close approximation of a circularly symmetric band-pass filter whose transfer function contains a pass region which is a ring of center frequency f_c and width $f_c/2$. The minimum stop-band attenuation is 4dB greater than that of the individual filters. Thus for $\beta = 3.68$, $A_c = -42.414 + 4\text{dB} = -38.414\text{dB}$ and $\delta = .0075 \times 4 = .030$. A plot of the transfer function for a circularly symmetric band pass filter for which $f_c = .15$ and $M_i=M_a=6$ is shown in Figure 3.2 below.

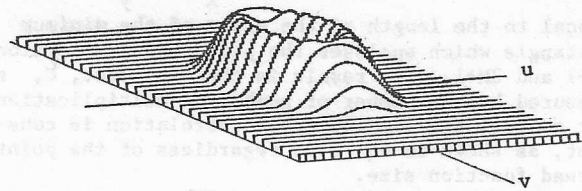


Figure 3.2 Transfer Function of Circularly Symmetric Band Pass Filter for which $f_c = .15$, $\Delta f = .20$, $M_i = M_a = 6$.

4.0 Experimental Evaluation

In this section we describe three simple experiments in which the filters derived in section 3 are used to detect classes of objects. The three 128×128 test images for these experiments, shown at the top of figure 4.1, have 256 grey levels. The first is an artificial image of circles of radius 6 and 8, with intensity 128 on a background of 64. Our task for this image is to detect the circles of radius 6 while avoiding the circles of radius 8.

The second test image is an artificial image containing a "herring bone" pattern. This pattern is composed of line segments of width 4, length 16, and a separation of 4 oriented at 45° and -45° . The pattern is of intensity 128 on a background of 32. The task for this image is to detect the -45° bars.

The third test image is taken from a digitized liver tissue biopsy image. Our task for this image is to detect the small dark nuclei of leukocytes and other cells in an inflammatory region at the top of the image while avoiding the nuclei of hepatic (liver) cells which are somewhat larger but often equally dark.

The filters used in these experiments have been normalized for a peak gain of 1 by dividing the point spread function by the square root of the sum of the squares of the coefficients. Prior to the computation of a correlation the mean and standard deviation of the picture points within the image are computed. During the computation of the correlation, as each picture element is read, it is converted to a 32 bit floating point number, the mean is subtracted, and the difference is multiplied by one over the standard deviation. Thus the resulting correlation is independent of the bias and gain at which the image was recorded.

The result of each sampled cross correlation is an array of floating point numbers. The maximum and minimum values in this array are determined and this range is divided into 256 bins, with the most negative value assigned to bin 0 and the most positive value assigned to bin 255. An integer block is then constructed in which the bin number from each value in the sampled correlation is written in a rectangle. The length of the sides of this rectangle are the horizontal and vertical sample rates (S_y and S_x). The rectangle is centered at the point at which that sampled correlation value was measured.

4.1 Object Detection Experiments

To detect the circles of radius 6 in the first test image we employed a circularly symmetric band pass filter of center frequency, $f_c = .15$. The point spread function duration of this filter approximates a circle of diameter 13. The Kaiser parameter for this filter was computed for $\Delta f = .20$ which resulted in $\beta = 3.68$. The cross correlation was sampled at horizontal and vertical sample rates of 2.

To detect the bars of -45° in the herring bone pattern we employed a directionally sensitive filter constructed over a circle of radius 4. The Kaiser low pass window was computed for $\Delta f = .25$ which resulted in a shape parameter of $\beta = 2.99$ and $A_t = -36.67$ dB. The low pass window was multiplied by a cosine of $f_c = .25$ and $\phi = -45^\circ$. Horizontal and vertical sample rates of 2 were used.

To detect the nuclei in the region of inflammation in the liver tissue we employed a circularly symmetric band pass filter of center frequency, $f_c = .25$. The Kaiser window was computed for $\Delta f = .25$ which gave a shape parameter of $\beta = 2.99$.

The spots which resulted from thresholding the mask constructed from the correlation are shown at the bottom of figure 4.1 as white spots superimposed over the original images. For the first two test images, the thresholds were set to the maximum bin,

i.e. 255. For the liver tissue image a threshold of 204 was used. This value was determined to be the optimal value during an experiment in which inflammatory regions were detected in 128 by 128 blocks in several tissue images from different patients.

5.0 Conclusions

The transfer function of a linear operator, derived in section two, has been found to be a powerful analytic technique for describing the effects of a linear operation on a digitized picture.

The family of filters derived in section three have been found useful for a variety of applications. A local average of the RMS output of several filters may provide a vector of features for classification of textured regions. Circularly symmetric band pass filters constructed from a sum of four angularly sensitive filters may be used to discriminate image objects on the basis of size. A sum of normalized orientation sensitive filters have been found to form a wedge filter which may be used to discriminate objects on the basis of orientation. The cross correlations of several orientation sensitive filters may be used to construct a symbolic description of objects in an image.

In section four we demonstrate the ability of specific filters to detect objects on the basis of size and orientation. Due to space limitations we were unable to report on the results of an experiment in texture segmentation based on the density of above threshold correlation spots.

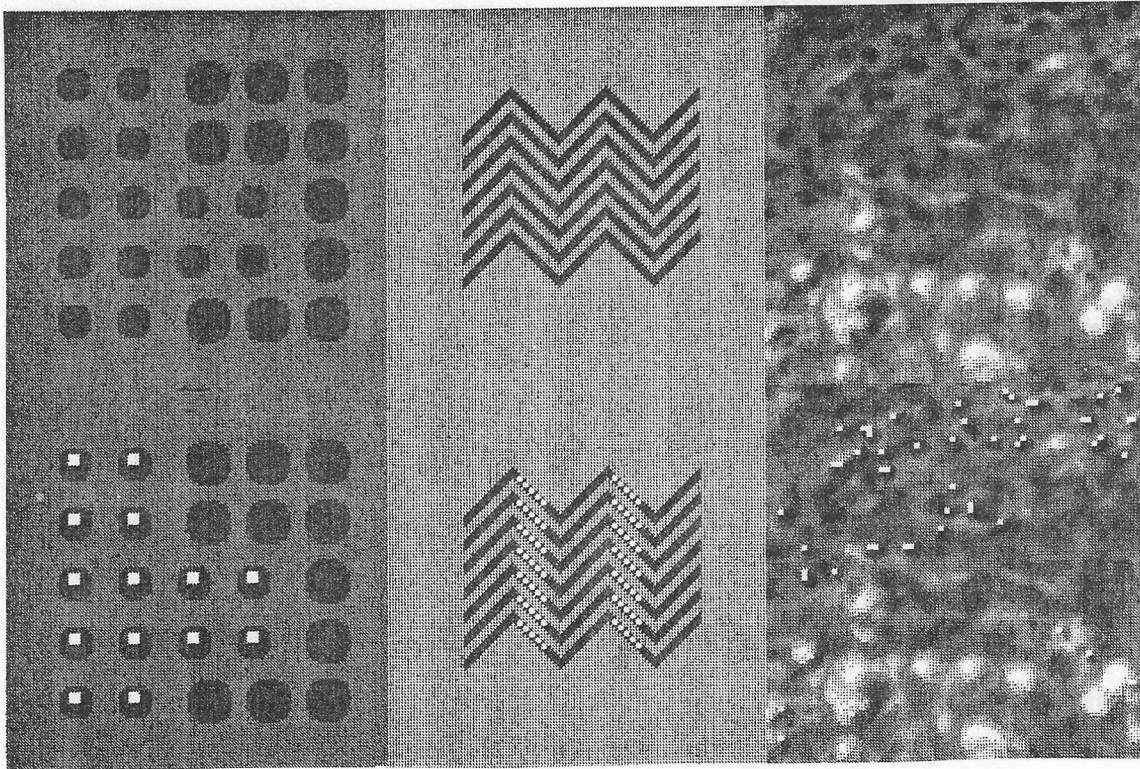


Figure 4.1 Three 128 Row By 128 Column Test Images (Top) and the Three Result Images (Bottom)

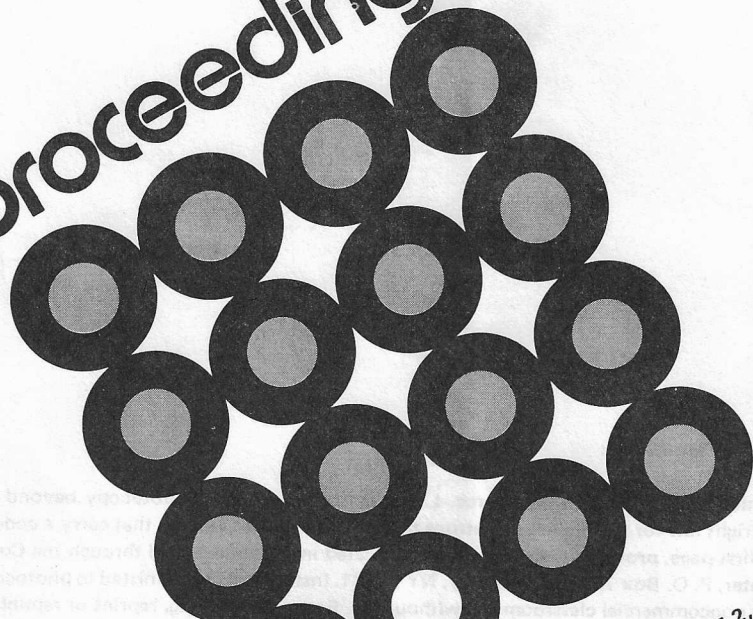
Acknowledgement:

This work was supported by NSF Grant APR76-09401 from the Research Applications directorate.

Bibliography:

- [1] Bajcsy, R., 1973, "Computer Description of Textured Surfaces", Proceedings of 3rd Int. Joint Conf. on Artificial Intelligence, pp. 572-579, Aug. 1973.
- [2] Duda, R.O. and P.E. Hart, 1973, Picture Processing and Scene Analysis, Wiley, New York.
- [3] Haralick, R.M., K. Shanmugan, and I. Dinstein, 1973, "Textural Features for Image Classification", IEEE Transactions on Systems, Man and Cybernetics, Nov. 1973.
- [4] Kaiser, J.F., 1974, "Nonrecursive Digital Filter Design Using the I_0 -Sinh Window Function" Proceedings of the 1974 IEEE International Symposium on Circuits and Systems, April, 1974.
- [5] Landau, H.J., and H.O. Pollack, 1961, "Prolate Spheroidal Wave Functions, Fourier Analysis, and Uncertainty - II", Bell Systems Technical Journal, Vol. 40, pp.65-84, Jan. 1961.
- [6] McClellan, J.H., T.W. Parks and L.R. Rabiner, 1973, "A Computer Program for Designing Optimum FIR Linear Phase Digital Filters", IEEE Transactions on Audio and Electroacoustics, Vol. AU-21, pp. 506-526, Dec. 1973.
- [7] Ohlander, R.B., 1975, "Analysis of Natural Scenes," Ph.D. Dissertation, Dept. of Computer Science, Carnegie-Mellon University.
- [8] Oppenheim, A.V. and R.W. Schaffer, 1975, Digital Signal Processing, Prentice Hall, New Jersey.
- [9] Papoulis, A., 1968, Systems and Transforms with Applications in Optics, McGraw Hill.
- [10] Parker, A. and J. Crowley, 1978, "Linear Analysis of Picture Processing Operators", COMPCON, Spring 1978, pp. 320-324.
- [11] Rabiner, L.R., and B. Gold, 1975, Theory, and Application of Digital Signal Processing, Prentice Hall Inc.
- [12] Rosenfeld, A., 1969, Picture Processing by Computer, Academic Press, N.Y.
- [13] Slepian, D. and H.O. Pollack, 1961, "Prolate Spheroidal Wave Functions, Fourier Analysis, and Uncertainty - I", Bell Systems Technical Journal, Vol. 40, pp. 43-63, Jan. 1961.

Proceedings



MAY 31-JUNE 2, 1978
CHICAGO, ILLINOIS

PR 78

IEEE Computer Society
Conference on


pattern
recognition
and
image
processing

78 CH1318-5C

Additional copies available from:

IEEE Computer Society
5855 Naples Plaza, Suite 301
Long Beach, California 90803

IEEE Service Center
445 Hoes Lane
Piscataway, NJ 08854

 Institute of Electrical and Electronics Engineers, Inc., New York, N.Y.,

IEEE COMPUTER SOCIETY CONFERENCE ON PATTERN RECOGNITION AND IMAGE PROCESSING

Conference Committee

Conference Co-Chairperson	K. S. Fu
Conference Co-Chairperson	B. McCormick
Technical Program Co-Chairperson	R. L. Kashyap
Technical Program Co-Chairperson	K. Preston
Local Arrangements Co-Chairperson	A. E. Akers
Local Arrangements Co-Chairperson	Y. P. Chien
Publication Chairperson	C. C. Li
Registration Chairperson	H. Wechsler

Program Committee

R. L. Kashyap, Co-Chairman
Ken Preston, Jr., Co-Chairman

Members

S. K. Chang
Y. T. Chien
H. Freeman
R. M. Haralick
T. Pavlidis
A. Rosenfeld
T. Wagner
G. White

1978 IEEE COMPUTER SOCIETY CONFERENCE
ON
PATTERN RECOGNITION AND IMAGE PROCESSING

Session Chairperson
and Banquet Speakers

Wednesday, May 31, 1978

Session WA1	Chairperson:	C. N. Liu, IBM
	Co-Chairperson:	C. K. Chow, IBM
Session WA2	Chairperson:	R. Kirsch, NBS
	Co-Chairperson:	H. Wechsler, Purdue
Session WA3	Chairperson:	L. Tubbs, BMDTC
Session WP1	Chairperson:	H. Andrews, USC
	Co-Chairperson:	B. McCormick, UICC
Session WP2	Chairperson:	Y. T. Chien, UC
Session WP3	Moderator:	R. L. Kashyap, Purdue

Thursday, June 1, 1978

Session TA1	Chairperson:	J. Sklansky, UCI
Session TA2	Chairperson:	H. Freeman, RPI
Session TA3	Chairperson:	T. Pavlidis, P.U.
Session TP1	Chairperson:	R. Haralick, U.K.
Session TP2	Chairperson:	T. Huang, Purdue
	Co-Chairperson:	E. Parker, CMU
Session TP3	Moderator:	K. Preston Jr., CMU

Banquet Speakers: Merlin Smith, President of IEEE Computer Society
A. Vacroux, IIT

Friday, June 2, 1978

Session FA1	Chairperson:	J. Tou, U. of Fla.
Session FA2	Chairperson:	A. Rosenfeld, U of Md.
Session FA3	Chairperson:	S. K. Chang, UICC
Session FP1	Chairperson:	C. L. Coates, Purdue
	Co-Chairperson:	N. Kaplan, NSF
Session FP2	Chairperson:	K. Preston Jr., CMU
Session FP3	Chairperson:	R. L. Kashyap, Purdue
Session FP4	Moderator:	G. White, ITT